

Maintenance of the International Celestial Reference Frame

S. Lambert, E. F. Arias

SYRTE, Observatoire de Paris, Université PSL, CNRS, Sorbonne Université, LNE
61 av. de l'Observatoire, 75014 Paris, France

Published in IERS annual report 2019

1. The international reference frame ICRF3

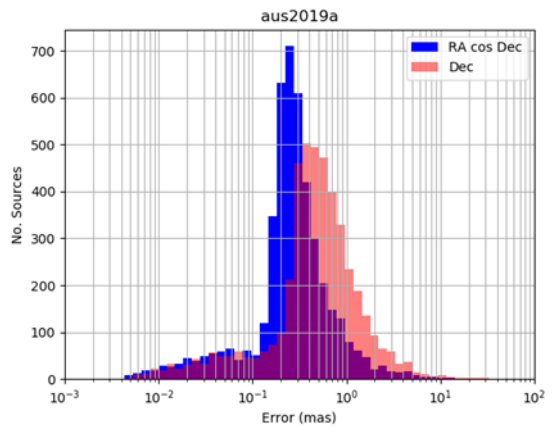
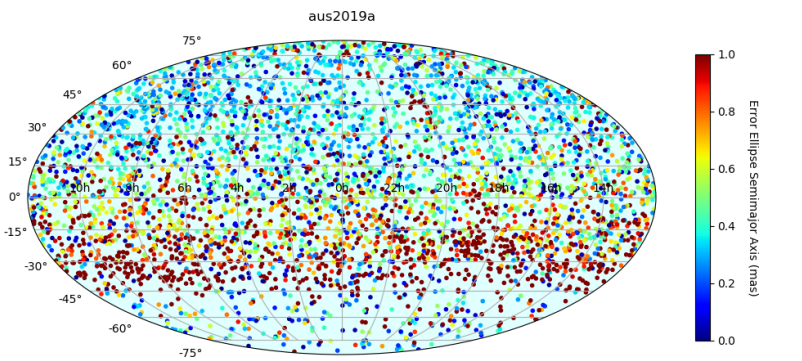
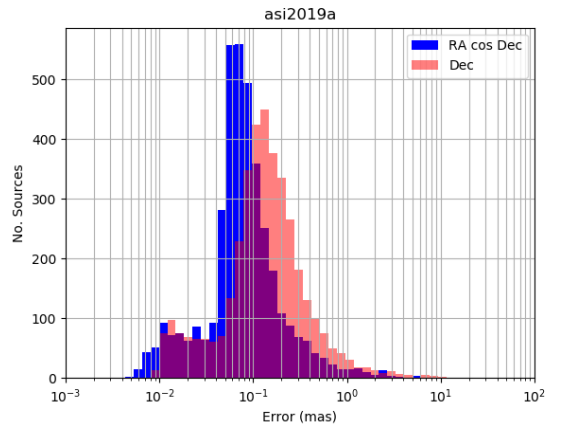
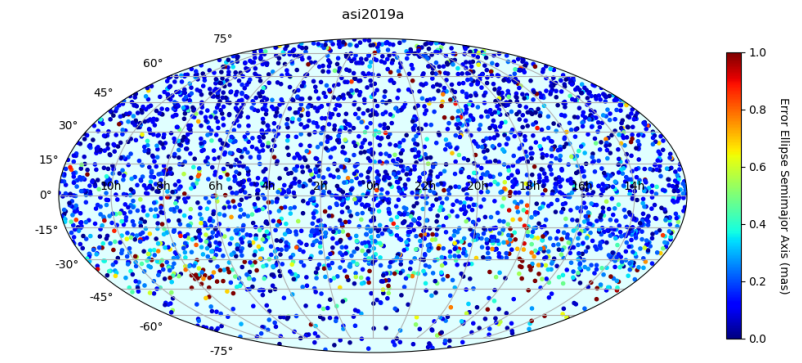
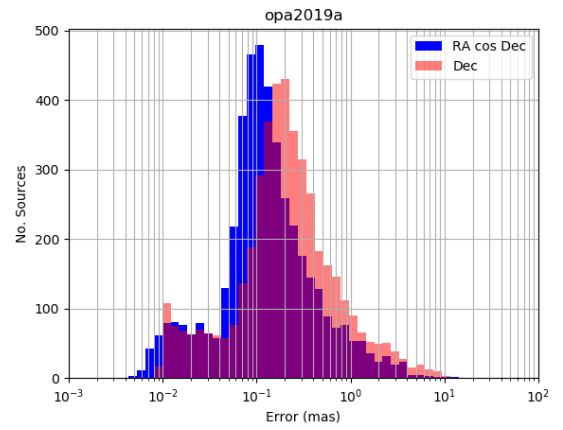
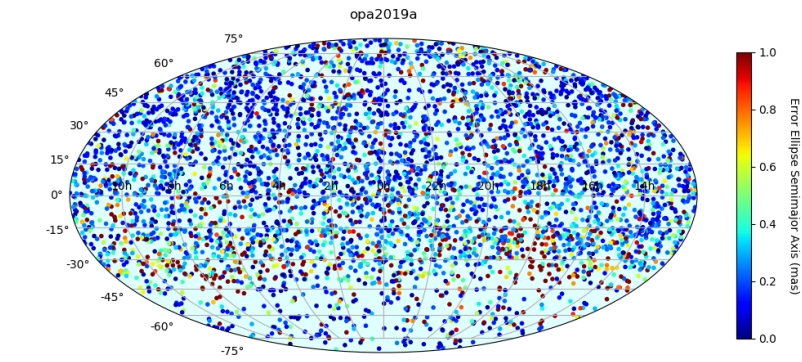
Resolution B2 of the XXX IAU General Assembly (IAU 2019) resolves that as from 1 January 2019 ICRF3 is the fundamental realization of the International Celestial Reference System (ICRS). This third representation of the International Celestial Reference System (ICRS) in radio wavelengths is a catalog of radio source positions described in Charlot et al. 2020. The ICRF3 consists in three catalogs at bands S/X, K and X/Ka with 4536, 824 and 678 objects respectively [<http://iers.obspm.fr/icrs-pc/newwww/icrf>].

Objects in the new frame had been used to orientate the second Gaia data release DR2 catalog onto the ICRS, as will be the case of the Gaia final catalog.

2. Monitoring of the ICRS

Monitoring the ICRS is a mission of the IERS ICRS Centre. This includes verifications of the stability of the axes of the system materialized through the frame, identification of the possible deformations of the frame and tracking the astrometric evolution of its defining sources. Another aspect of this activity consists on the analysis of individual solutions submitted by the VLBI analysis centres to the International VLBI Service (IVS).

The IERS ICRS Centre at Paris Observatory developed the tools for determining the orientation of the axes, characterizing the deformations of the frame and analyzing the astrometric quality of radio source positions (Lambert 2014). For this report analyses with respect to the conventional reference ICRF3 are presented, as well as with respect to Gaia DR2, which constitutes a preliminary version the catalog that will allow the access to ICRS in optical wavelengths.



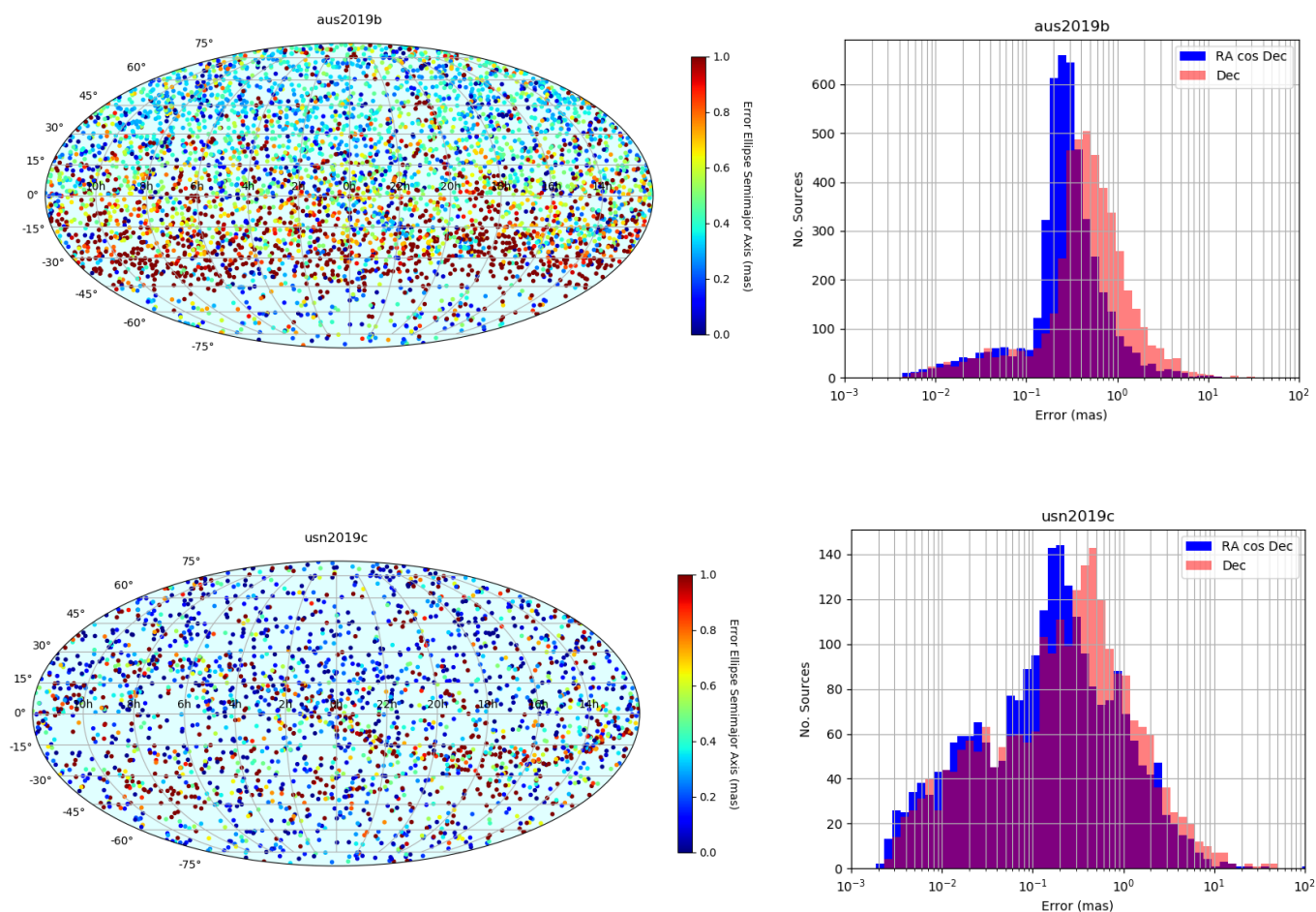


Figure 1. Left: sky distribution of the catalogs highlighting the overall positional error computed as the major axis of the error ellipse. Right: distribution of the standard errors on source position.

3. Analysis of recent VLBI catalogs

3.1. Data

We analyzed five catalogs submitted to the IVS in 2019. The catalogs were respectively submitted by the Space Geodesy Centre of the Italian Space Agency (ASI/CGS; solution asi2019a), by Geoscience Australia (aus2019a and 2019b), by Paris Observatory (opa2019a) and by the Unites States Naval Observatory (usn2019c). The two solutions aus2019a and aus2019b were obtained with the OCCAM geodetic VLBI analysis software package (Titov et al. 2004), whereas the other four catalogs were obtained with Calc/Solve (Ma et al. 1986).

The catalogs were released after the date of adoption of the ICRF3, therefore their individual frames had been oriented on ICRF3 by applying no net rotation constraints, with the exception of the ASI solution, which has been oriented onto ICRF2. Positions in ICRF3 had been adopted for the a priori catalogs in the solutions, with the exception of ASI, where the a priori source positions are the ICRF2

coordinates. In our analysis we have compared these individual solutions to the catalog representing ICRF3 in the S/X bands (ICRF3X in this report). The 2983 sources in common between the ICRF3 and the second Gaia data release (DR2; Prusti et al. 2016; Brown et al. 2016, 2018; Mignard et al. 2018) have been used also as a reference for comparison.

3.2. Overview of the catalogs

The number of sources in each catalog, the mean epoch of the observations, and the median positional errors (for RA cos DEC, Dec, and for the error ellipse major axis) are reported in Table 1. The standard error of the catalog positions differs in the solutions; the smallest values from ASI may depend on the choice of very good sources, AUS positions might be influenced by a large number of sources with errors in the range 0.6 – 1 mas in the Southern hemisphere. The USN solution did not consider a number of ‘special’ sessions including VCS sessions and provide therefore coordinates for a relatively small number of sources.

	N	Epoch	E_RA*	E_Dec	E_EEMA
opa2019a	4468	2010.93	116.90	196.55	205.89
aus2019a	4529	2012.71	261.57	478.00	496.19
aus2019b	4645	2012.96	273.72	471.20	493.59
asi2019a	3850	2013.78	74.98	130.80	133.37
usn2019c	2390	2012.01	171.77	259.80	289.09

Table 1. Statistic information of the catalogs here reported. N is the number of sources. The mean epoch corresponds to the average of the mean observational epochs of each source. N is the number of sources, E_RA*, E_Dec are respectively the median standard errors in right ascension (scaled by cos dec) and in declination, E_EEMA is the median major axis of error ellipses. Unit is μas .

The sky distribution of the radio sources in each catalog is plotted in Fig. 1 together with the distribution of the standard errors. In the sky maps, the color indicates the overall error computed as the major axis of the error ellipse, calculated using the correlation information between the coordinates as provided in the catalogs.

Fig. 2 presents three plots; on top the error distribution, including that of the catalogs used as reference in the comparisons (ICRF3X and Gaia DR2); at the bottom the dependence of the error on the declination including the common sources to all catalogs (left) and all sources in each catalog (right) are displayed for which we took the running median error within windows of 15° .

The plots show a clear declination-dependent error for the individual catalogs. When sources common to all catalogs are considered, the behavior of the VLBI solutions is similar, peaking at about -30° declination, and reaching small error values around $+45^\circ$ declination, certainly due to the presence of a substantial number of good astrometric common sources in that region. This effect is not visible in the plot where all sources in each catalog are considered. Both AUS solutions show the largest errors, particularly at mid- latitudes in the Southern hemisphere, very probably due to the network asymmetry and the quality of the sources in the South, visible in the plots of Fig. 1. The Gaia scanning law allows to cover both hemispheres symmetrically, and in consequence the Gaia DR2 catalog does not show such systematic effects.

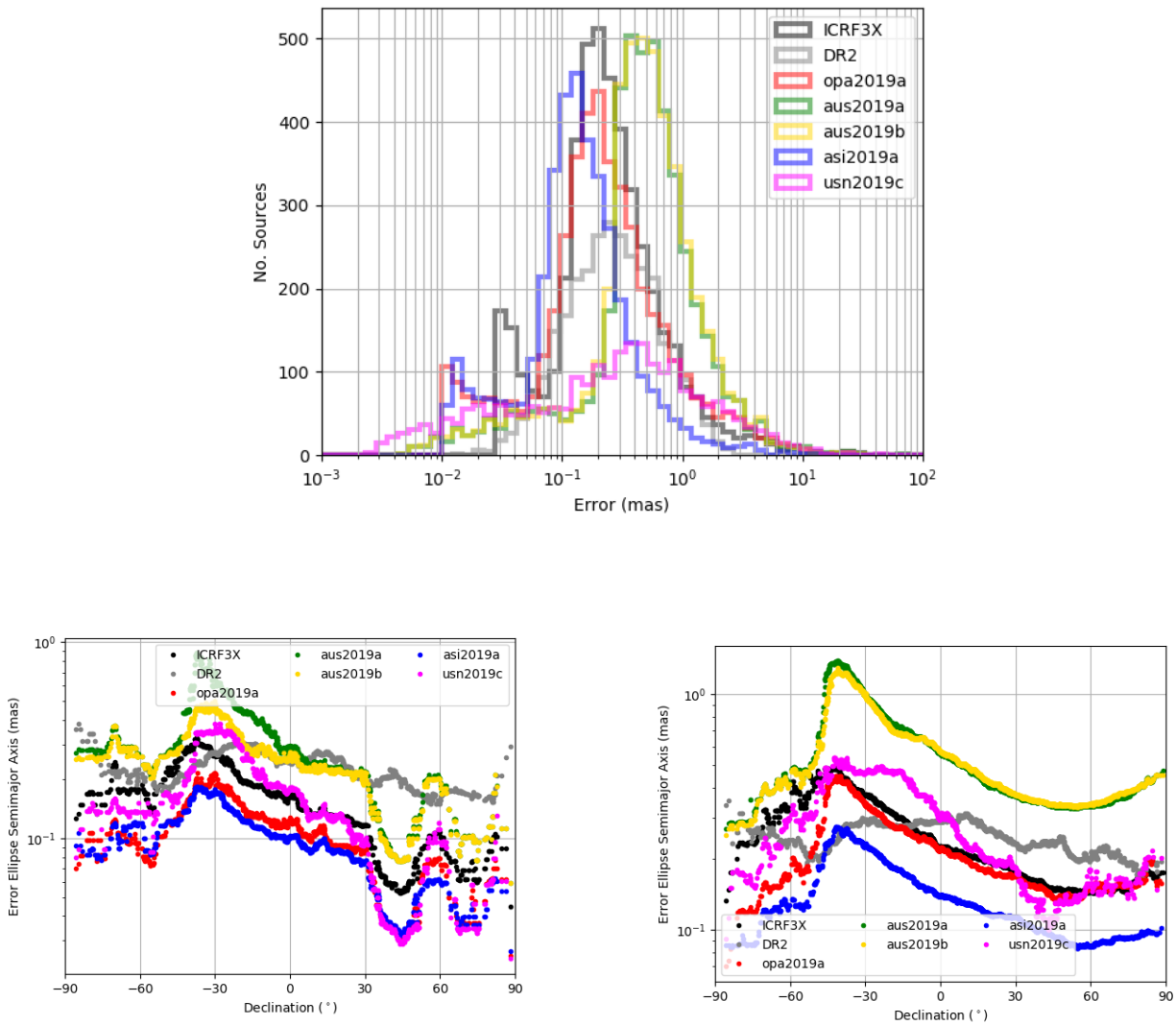


Figure 2. Top: overall comparison of the standard error distribution. Bottom: standard errors in source positions as a function of the declination smoothed by taking the running median within bins of 15 degrees, for sources common to all catalogs (left) and for all sources in each catalog (right).

3.3. Comparison with ICRF3 and Gaia DR2

Figure 3 displays the differences in declination between the catalogs and the references averaged within bins of 200 sources in two configurations: all sources (left) and sources common to all catalogs (right). Most deformations are smaller than $50 \mu\text{as}$ when the differences with respect ICRF3X are computed with all the sources in each catalog (top left), only the AUS solutions present effects close to 0.1 mas between 0° and -30° , probably due to the network geometry and the quality of sources at negative declinations. Deformations are smoother when the differences are computed with common sources (top right), they remain within less than $40 \mu\text{as}$. The amplitude of the deformations is bigger when the differences are computed with respect to Gaia DR2, since the sphere of Gaia is in principle not affected by deformations.

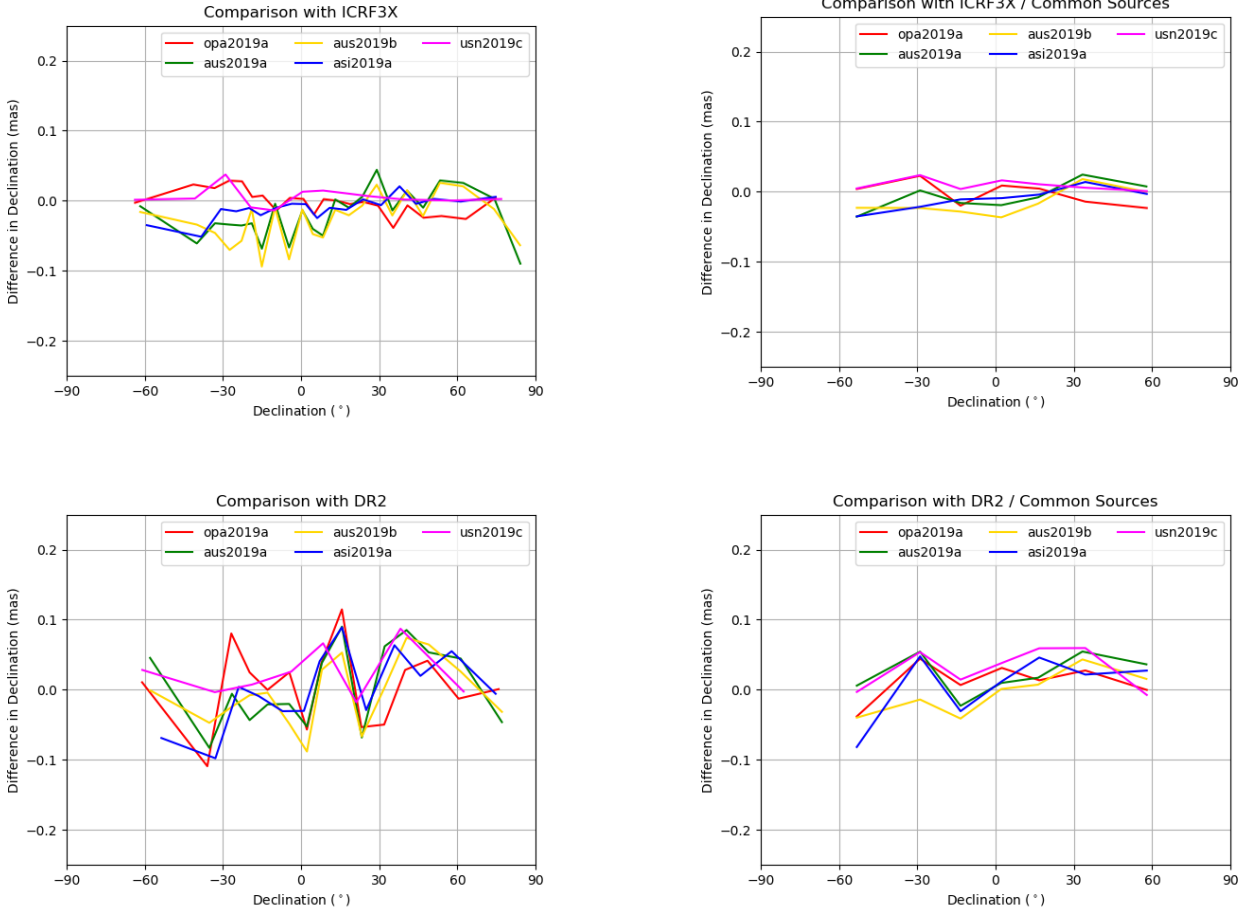


Figure 3. Differences in declination between the catalogs and the references (ICRF3X: top; Gaia DR2, bottom) averaged in bins of 200 sources sorted by declination for all sources (left) and for common sources to all catalogs (right).

Catalog comparisons had been computed using the 16-parameter transformation accounting for rotations around the three axes, a glide, and degree-2 electric- and magnetic-type deformations (see e.g., Mignard and Klioner 2012). The coordinate differences $\Delta\alpha$ and $\Delta\delta$ between a catalog and a reference catalog read

$$\begin{aligned}
 \Delta\alpha \cos \delta &= R_1 \cos \alpha \sin \delta + R_2 \sin \alpha \sin \delta - R_3 \cos \delta - D_1 \sin \alpha + D_2 \cos \alpha + M_{20} \sin 2\delta \\
 &+ (E_{21}^{\text{Re}} \sin \alpha + E_{21}^{\text{Im}} \cos \alpha) \sin \delta - (M_{21}^{\text{Re}} \cos \alpha - M_{21}^{\text{Im}} \sin \alpha) \cos 2\delta \\
 &- 2 (E_{22}^{\text{Re}} \sin 2\alpha + E_{22}^{\text{Im}} \cos 2\alpha) \cos \delta - (M_{22}^{\text{Re}} \cos 2\alpha - M_{22}^{\text{Im}} \sin 2\alpha) \sin 2\delta, \\
 \Delta\delta &= -R_1 \sin \alpha + R_2 \cos \alpha - D_1 \cos \alpha \sin \delta - D_2 \sin \alpha \sin \delta + D_3 \cos \delta + E_{20} \sin 2\delta \\
 &- (E_{21}^{\text{Re}} \cos \alpha - E_{21}^{\text{Im}} \sin \alpha) \cos 2\delta - (M_{21}^{\text{Re}} \sin \alpha + M_{21}^{\text{Im}} \cos \alpha) \sin \delta \\
 &- (E_{22}^{\text{Re}} \cos 2\alpha - E_{22}^{\text{Im}} \sin 2\alpha) \sin 2\delta + 2 (M_{22}^{\text{Re}} \sin 2\alpha + M_{22}^{\text{Im}} \cos 2\alpha) \cos \delta,
 \end{aligned}$$

where α and δ are the coordinates of the object in the reference catalog. We used weighted least-squares to solve the system, with weights computed using the available covariance information (i.e., the standard errors on individual source coordinates and their correlation). The values of the

transformation parameters adjusted to the catalogs compared to the ICRF3X and Gaia DR2 and their standard errors are reported in Fig. 4 for two different set of sources, those common to all catalogs and each reference, and those common between each catalog and the reference. The resulting statistics after removal of systematics are reported in Table 2. Fig. 4 reveals that the results are similar independently from the set of sources used for the comparisons. The comparisons with ICRF3X show rotations of about 50 μas around the x and y axes for the OP and ASI solutions, and no significant deformations in all cases. Gaia DR2 has been oriented onto ICRF3, and we could expect no significant rotation between its axes and the VLBI solutions; this is the case, since the significant rotations in the plot correspond the OP and ASI solutions, rotated with respect to ICRF3X. Deformations are visible dependent on declination, consistently with Fig. 2.

Galactic aberration has been accounted for at the construction of ICRF3. Uncorrected Galactic aberration should provoke a glide of amplitude close to 5 $\mu\text{as/yr}$ (e.g., Kovalevsky 2003; Titov et al. 2011) towards the Galactic center (approx. R.A. 265° and declination -29°). A value of 5.8 $\mu\text{as/yr}$ for the amplitude of the Galactic aberration has been evaluated in analyses performed at the construction of the ICRF3 (MacMillan et al. 2019). The descriptions of the solutions provided to the IVS used in this report indicate that this correction has been applied in the OP and AUS solutions (for details refer to <http://ivsopar.obspm.fr/vlbi/ivsproducts/crf/>). The effect of uncorrected Galactic aberration in the other solutions is not clearly visible in the deformation parameters since the mean epochs of the catalogs are close to that of ICRF3 (2015.0) and Gaia DR2 (2015.5).

Table 2. Statistics of the differences of the catalogs to ICRF3X and Gaia DR2 with different sets of common sources, and after removal of large-scale systematics. RA* stands for RA cos_dec. Unit is μas .

2a. With respect to ICRF3X, N: number of sources common to ICRF3X and each individual catalog.

	N	Std_RA*	Std_Dec	Chi2_RA*	Chi2_Dec	Std_RA*	Std_Dec	Chi2_RA*	Chi2_Dec
opa2019a	4381	76.52	92.83	0.71	0.75	73.31	82.92	0.65	0.60
aus2019a	4433	107.19	122.07	0.83	0.83	106.91	121.40	0.83	0.82
aus2019b	4434	110.68	121.56	0.90	0.84	109.92	120.55	0.88	0.82
asi2019a	3799	69.00	84.52	0.68	0.71	66.05	75.36	0.62	0.57
usn2019c	2274	62.83	63.88	0.81	0.68	62.74	63.61	0.81	0.67

2b. With respect to ICRF3X, N: number of sources common to all catalogs.

	N	Std_RA*	Std_Dec	Chi2_RA*	Chi2_Dec	Std_RA*	Std_Dec	Chi2_RA*	Chi2_Dec
opa2019a	1375	50.55	66.06	0.67	0.89	45.79	51.35	0.55	0.54
aus2019a	1379	69.70	75.32	0.90	0.87	69.21	74.37	0.89	0.85
aus2019b	1379	71.81	75.92	0.97	0.90	70.77	74.40	0.94	0.86
asi2019a	1375	53.85	65.40	0.76	0.85	49.81	53.00	0.65	0.56
usn2019c	1375	53.90	54.19	0.77	0.63	53.79	53.90	0.76	0.62

2c. With respect to Gaia-DR2, N: number of sources common to DR2 and each individual catalog.

	N	Std_RA*	Std_Dec	Chi2_RA*	Chi2_Dec	Std_RA*	Std_Dec	Chi2_RA*	Chi2_Dec
opa2019a	2912	301.75	316.07	2.44	2.37	298.93	311.05	2.39	2.30
aus2019a	2920	354.26	355.35	2.10	1.73	352.41	353.16	2.08	1.71
aus2019b	2920	356.79	353.53	2.14	1.76	354.80	350.80	2.12	1.73
asi2019a	2525	263.54	286.96	2.41	2.48	262.29	283.17	2.39	2.41
usn2019c	1596	262.69	263.91	2.30	2.27	260.82	262.14	2.27	2.24

2d. With respect to Gaia-DR2, N: number of sources common to all catalogs.

	N	Std_RA*	Std_Dec	Chi2_RA*	Chi2_Dec	Std_RA*	Std_Dec	Chi2_RA*	Chi2_Dec
opa2019a	1375	261.61	262.76	2.54	2.56	258.68	256.66	2.49	2.45
aus2019a	1379	291.64	285.37	2.36	2.09	288.84	281.43	2.31	2.04
aus2019b	1379	288.29	287.63	2.35	2.20	285.41	282.94	2.30	2.13
asi2019a	1375	245.37	253.55	2.45	2.49	243.96	248.34	2.43	2.38

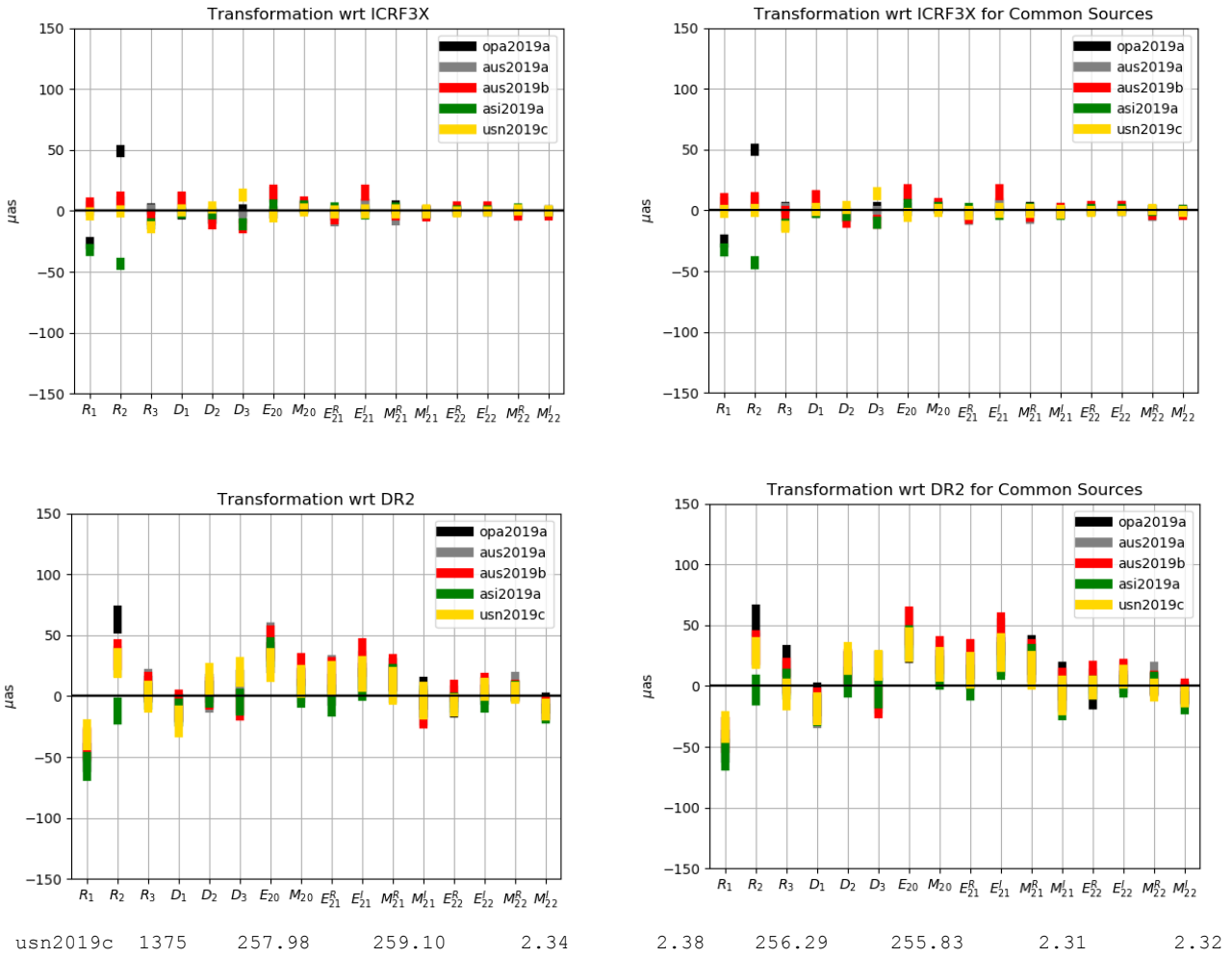


Figure 4. Transformation parameters between the catalogs under analysis and the reference frames (ICRF3X: top, Gaia DR2: bottom). The plots on the left represent parameters computed with sources common to each individual catalog and the frame used as reference (from top to bottom they correspond to the statistics in tables 2a and 2c); the plots on the right represent parameters computed with sources common to all the catalogs involved in the comparisons, including the references (from top to bottom they correspond to the statistics in tables 2b and 2d).

3.4. Conclusions and recommendations

Five individual catalogs submitted to the IVS in 2019 are analyzed in this report. The axes of their frames are consistent with ICRF3X at the level of $50 \mu\text{as}$ without any zonal deformation beyond $15 \mu\text{as}$. This result is also valid for the ASI solution, which has been aligned to ICRF2, confirming the good consistency between ICRF2 and ICRF3. Compared to Gaia DR2, a similar misalignment, of order $50 \mu\text{as}$ is visible, with significant zonal deformations particularly for the AUS solutions.

For a better evaluation of the consistency of the VLBI products and a better maintenance of the reference frame, we request analysis centres to submit solutions aligned to the new reference ICRF3, as well as to adopt the ICRF3 catalogue for the a priori positions in the solutions. In all solutions the correction for the amplitude of the Galactic aberration must be implemented using the recommended value. These catalogs should be as complete as possible, i.e., processing as much VLBI sessions as

possible since 1979. Analysis strategies should be rigorously documented and motivated. The main points that will be scrutinized in the next reports will be the zonal systematics, their relation with the Galactic aberration, and the agreement with the current (DR2) and future releases of Gaia.

4. References

A. G. A. Brown, A. Vallenari, T. Prusti, J. H. J. de Bruijne, F. Mignard, R. Drimmel, C. Babusiaux, C. A. L. Bailer-Jones, U. Bastian, et al. Gaia Data Release 1. Summary of the astrometric, photometric, and survey properties. *Astronomy & Astrophysics*, 595:A2, Nov. 2016.

A. G. A. Brown, A. Vallenari, T. Prusti, J. H. J. de Bruijne, C. Babusiaux, C. A. L. Bailer-Jones, M. Biermann, D. W. Evans, L. Eyer, et al. Gaia Data Release 2. Summary of the contents and survey properties. *Astronomy & Astrophysics*, 616:A1, Aug. 2018.

P. Charlot, C. S. Jacobs, D. Gordon, S. B. Lambert, J. Boehm, A. de Witt, A. Fey, R. Heinkelmann, E. Skurikhina, O. Titov, E. F. Arias, S. Bolotin, G. Bourda, C. Ma, Z. Malkin, A. Nothnagel, R. A. Gaume, D. Mayer, and D. S. MacMillan. The third realization of the International Celestial Reference Frame by very long baseline interferometry. *Astronomy & Astrophysics*, (in press), 2020.

International Astronomical Union. Transactions IAU, Vol. XXXB, Proc. of the XXX IAU General Assembly, August 2018 (Ed. Teresa Lago), 2019.

J. Kovalevsky. Aberration in proper motions. *Astronomy & Astrophysics*, 404:743–747, June 2003.

S. Lambert. Comparison of VLBI radio source catalogs. *Astronomy & Astrophysics*, 570:A108, 2014

C. Ma, T. A. Clark, J. W. Ryan, T. A. Herring, I. I. Shapiro, B. E. Corey, H. F. Hinteregger, A. E. E. Rogers, A. R. Whitney, C. A. Knight, G. L. Lundqvist, D. B. Shaffer, N. R. Vandenberg, J. C. Pigg, B. R. Schupler, and B. O. Ronnang. Radio-source positions from VLBI. *Astronomical Journal*, 92:1020–1029, Nov. 1986.

D.S. MacMillan, A. L. Fey, J. M. Gipson, D. Gordon, C. S. Jacobs, H. Krásná, S. Lambert, Z. Malkin, O. A. Titov, G. Wang, and M. H. Xu, Galactocentric acceleration in VLBI analysis - Findings of IVS WG8, *Astronomy and Astrophysics*, 630:A93, 2019

F. Mignard and S. Klioner. Analysis of astrometric catalogues with vector spherical harmonics. *Astronomy & Astrophysics*, 547:A59, 2012.

F. Mignard, S. A. Klioner, L. Lindegren, J. Hernandez, U. Bastian, A. Bombrun, D. Hobbs, U. Lammers, D. Michalik, et al. Gaia Data Release 2. The celestial reference frame (Gaia-CRF2). *Astronomy & Astrophysics*, 616:A14, 2018.

T. Prusti, J. H. J. de Bruijne, A. G. A. Brown, Vallenari, A., Babusiaux, C., Bailer-Jones, C. A. L., Bastian, U., Biermann, M., Evans, D. W., et al. The Gaia mission. *Astronomy & Astrophysics*, 595:A1, 2016.

O. Titov, V. Tesmer, and J. Boehm. OCCAM v.6.0 Software for VLBI Data Analysis. In N. R. Vandenberg and K. D. Baver, editors, *International VLBI Service for Geodesy and Astrometry 2004 General Meeting Proceedings*, page 267, June 2004.

O. Titov, S. B. Lambert, and A.-M. Gontier. VLBI measurement of the secular aberration drift. *Astronomy & Astrophysics*, 529:A91, May 2011.